UNIVERSITY OF OKLAHOMA

RESEARCH INSTITUTE

PROJECT 87

TECHNICAL REPORT

to

OFFICE OF NAVAL RESEARCH

Project Number NR 061 078
Contract Number N onr 982(02)

ONE-DIMENSIONAL FLUID FLOW PRODUCED BY CONFINED SPARKS*

BY

WILLIAM R. ATKINSON

TECHNICAL REPORT

TO

OFFICE OF NAVAL RESEARCH

Contract Number Nonr 982(02)

---

*This report summarizes a thesis submitted to the Graduate Faculty of the University of Oklahoma in partial fulfillment of the requirement for the degree of Doctor of Philosophy.

ONE-DIMENSIONAL FLUID FLOW PRODUCED BY CONFINED SPARKS

CHAPTER I

INTRODUCTION

Common experiences ranging from witnessing a thunder storm to combing one's hair demonstrate that one of the prominent features of the spark discharge is the conversion of electrical energy into sound energy. Quite often sparks are audible even though they are scarcely visible. The early investigators, A. Toepler,[1] Mach,[2] Dvorak,[3] M. Toepler,[4] and Foley,[5] studied the shock waves or large amplitude sound pulses produced by unconfined sparks at atmospheric pressure, but it appears that few if any have studied the plane shock fronts one would expect to be produced by allowing spark heated gas to expand in only one direction. Such a study could certainly be made more complete than a similar study with unconfined sparks.

About 1945, Rayleigh[6] and Zanstra[7] discussed certain non-shock aspects of an experiment performed by Rayleigh in which an electrical current was passed through part of a low pressure gas confined to a discharge tube designed to allow the discharge heated gas to expand unidirectionally into

that region of the tube which was not in the current path. With experimental conditions similar to Rayleigh's, one often observes that the heated gas first becomes brilliantly luminous and then that the luminous region expands into the portion of the discharge tube which is not directly in the current's path. Throughout the expansion, which often continues after the current has ceased, it does perhaps seem plausible that the luminous gas is simply the gas which was initially heated by the electrical current; however, this hypothesis is by no means obvious. The idea here expressed can be rephrased by asking if there is a non-diffusional flux of gas across the front of expanding luminosity or by asking if the expansion velocity of the initially heated gas coincides with the expansion velocity of the luminosity. Now under certain conditions, a thin front of luminosity precedes the main body of expanding luminosity, and under still other conditions the entire luminosity does not appear to expand at all but rather to move as a slug down the expansion chamber. The question posed in this paragraph is particularly pertinent when the Rayleigh phenomenon takes either of the last two forms.

The general problem of this thesis is one of examining the role of shock waves in electrical discharges similar to Rayleigh's, with a hope of explaining the time and position variation of the emitted luminosity. Attention will be focused on answering the question of the previous paragraph

by the methods of mechanics. Other methods, as for instance one based on the Doppler effect, will be considered in reference only.

Since 1948, the Rayleigh phenomena has been studied by numerous researchers working in collaboration with Fowler.[8,9,10,11] Goldstein[12] first observed the reflected luminous fronts which were studied in greater detail by Compton.[13] Lee[14] verified some of the experiments of Rayleigh and perfected the rotating mirror camera used in studying the motion of the luminous fronts. Clotfelter,[15] Atkinson,[16] Marks,[17] Kleider,[18] Rose,[19] and Coleman[20] have studied the discharge spectrographically to obtain several different types of information. For example, the Doppler effect has been used to determine velocities, and the Holtsmark theory of Stark broadening has been used to yield information about ion concentrations in the discharge. In addition, the spectrograms have yielded the usual information about the degree and extent of excitation for both pure gases and gas mixtures.

The recent increase of interest in the field of shock waves and compressible fluid flow is evident upon looking at the two hundred article bibliography given in Courant and Friedrichs' well known book,[21] which even so does not claim to contain a comprehensive bibliography of the recent literature. About two thirds of the listed references have been published since 1940.

A helpful description of shock tube operation given by Geiger, Mautz, Hollyer, and Laporte[22] was used along with Courant and Friedrichs' book in forming a basic theory of the Rayleigh phenomenon. Literature in the subfields of ionizing shocks and shocks in ionized gases is particularly pertinent to a complete study of the discharge. In 1920 Einstein[23] pointed out that sound propagated in partially dissociated gases exhibits dispersion phenomena because of the lag in establishing dissociation equilibrium. Suits[24] reported after analyzing experimental data, that dissociation equilibrium was probably not attained behind the shock fronts moving through the arcs he studied. Systematic methods of obtaining the thermodynamic properties of hot partially dissociated gases by means of partition functions have helped Brinkley, Kirkwood, and Richardson[25] in constructing the Hugoniot curve for air under atmospheric conditions. Resler, Lin, and Kantrowitz[26] gave similar information for argon at several different pressures. Their results were obtained by approximating the actual thermodynamic properties of argon by the properties of a Saha gas. In the last two papers it was assumed that dissociative equilibrium is achieved behind the shock front. Williamson[27] has studied the contribution of Coulomb interactions to the thermodynamic properties of a completely ionized gas under solar conditions, but as yet, the shock and fluid flow consequences of the Coulomb interactions, as they contribute to thermodynamic

properties, has hardly been studied at all. Late in 1951 Dennisse and Rocard[28] considered a somewhat different Coulomb produced effect associated with a shock's passage through an ionized gas. In their paper it is suggested that the origin of intense solar radio emission lies in the plasma oscillations promoted by the shock's existence.

CHAPTER II

GENERAL DESCRIPTION OF THE DISCHARGE AND THE EXPANSION PROCESS

Several styles of the discharge tube are suitable for producing the Rayleigh phenomenon; however, the various tube styles all have the functional similarity of possessing an expansion chamber and a heating or compression chamber. The glass or plastic tube from which both chambers are constructed usually has a diameter between 5 and 30 mm and is ordinarily gas filled to about 10 mm of Hg pressure. Historically the compression chamber described by Rayleigh was loop shaped so that the gas could be heated by electromagnetic induction of energy from a nearby oscillating circuit; however, a compression chamber with electrodes may also be used to permit more easily made measurements of the energy delivered to the tube. When electrodes are used with a 10 cm separation, approximately 10 joules of energy may be delivered to the tube by connecting it to a 15 μfd capacitor previously charged to 4000 volts. Within 5 μseconds the current rises to about 5000 amperes, and within 20 μseconds the current has usually decreased to a negligible value. During the discharge the entire compression chamber becomes

luminous and, as time progresses, more and more of the expansion chamber becomes luminous. Even after the current has subsided, the luminosity continues to advance at approximately 10^5 cm/sec for a total distance of perhaps 20 cm.

In order to continue this description of the luminosity motion, its qualitative similarity to gas flow in a conventional diaphragm shock tube will be noted.

In an ordinary shock tube after the rupture of the diaphragm separating the two pressure regions, a shock wave forms in the low pressure gas and moves through this gas leaving in its wake a region having a uniform pressure intermediate to the two initial pressures. In certain cases this pressure plateau may extend back into the compression chamber. Behind the shock in this region of uniform pressure the gas has a flow velocity somewhat less than the supersonic shock velocity U. The contact surface, the boundary between the gas initially present in the compression chamber on one side of the diaphragm and the gas originally present in the expansion chamber on the other side of the diaphragm, divides the region of uniform pressure and flow velocity into two subregions which differ in both temperature and specific volume. Some distance behind the contact surface lies the rarefaction wave, the pressure transition zone of finite thickness in which pressure and flow velocity vary with position monotonically and continuously. At the head or high pressure end of the rarefaction wave back in the compression

chamber the pressure is the initial compression chamber pressure and the flow velocity is zero. The qualitative description of the early state of affairs in the shock tube is completed by remarking that the gas at each point in the compression chamber is undisturbed by the breaking of the diaphragm until the head of the rarefaction wave, moving with local sound velocity, arrives at that point. Later phases of the flow pattern are marked by reflections of the shock and the rarefaction waves and the subsequent interaction between reflected fronts and advancing waves.

Returning now to the Rayleigh phenomena, we can observe many clues indicative of the shock tube behavior outlined above with photographic techniques alone. First of all, under certain conditions it is possible to recognize two distinct fronts of luminosity moving down the tube even when the electrical discharge is aperiodic. These two fronts differ in brilliance and velocity, and may be identified as a shock front and a slower contact surface. Under other conditions the luminosity advances as a single front whose velocity may be reversed by placing a piston in the expansion chamber. Sometimes this reflection occurs without the luminous fronts even reaching the piston. When the reflection occurs in this fashion, one may tentatively identify the luminous front as a contact surface preceded by a non-luminous shock which actually does reflect at the piston surface. It is this receding shock that then meets the advancing luminous front

and reverses the flow velocity of the luminous gas. In those cases in which there is only one luminous front and this front does reach the piston before reflecting, consistent use of the shock tube model would lead one to identify the luminous front as the shock itself, followed by a non-luminous contact surface. Observed luminous fronts that start at the piston in the expansion chamber and move toward the compression chamber may actually be shocks which start out at the compression chamber and only become intense enough to excite the gas after reflection from the piston. It is well known that the temperature behind a reflected shock is considerably greater than the temperature behind the same shock before reflection.

The correctness of the identification hypothesis above, indicated by purely qualitative evidence, can be substantially verified quantitatively by determining the velocity U of the hypothesized non-luminous shocks and by using this velocity U to compute the accompanying gas flow velocity u*, which can then be compared with observed luminosity velocities u. These measurements and computations were made and they will be discussed after first obtaining the formula relating shock and flow velocities.

CHAPTER III

THE RELATIONSHIP BETWEEN SHOCK AND FLOW VELOCITIES IN THE PRESENCE OF SHOCK-PRODUCED IONIZATION

Consider a strong ionizing shock moving into an un-ionized gas at rest. The shock imparts to the gas a flow energy, an internal kinetic energy commonly referred to as random thermal energy of motion, and an internal potential energy such as ionizational energy. For a monatomic gas a relationship between the shock velocity U, the gas flow velocity u_1, and the specific internal potential energy w produced by the shock will be found. The specific internal energy e will be approximated by equation (1).

$$e = 3p\tau/2 + w \tag{1}$$

The shock conditions are given by equations (2), (3), (4), and (5) in which the subscript 1 refers to the wake side of the shock and the subscript 0 refers to the other side.

$$(U-u_1)/\tau_1 = U/\tau_0 \tag{2}$$

$$p_1 + (U-u_1)^2/\tau_1 = p_0 + U^2/\tau_0 \tag{3}$$

$$(p_1+p_0)(\tau_0-\tau_1)/2 = e_1-e_0 \tag{4}$$

$$s_1-s_0 > 0 \tag{5}$$

where p is the pressure, τ is the specific volume, and s is the specific entropy. Since the gas is assumed to be un-ionized

on the 0 side of the shock, e_0 will be given by $3p_0\tau_0/2$; whereas e_1 will be given by $3p_1\tau_1/2 + w$. After eliminating p_1 and τ_1, replacing $5p_0\tau_0/3$ by the square of the sound speed c_0, and using definition (6), one obtains equation (7).

$$u^* = 3(U-c_0^2/U)/4 \tag{6}$$

$$u_1^2 - u^*u_1 - w/2 = 0 \tag{7}$$

From (7) we see that u* is the flow velocity behind a shock in a monatomic gas that does not acquire internal potential energy when passed over by a shock having velocity U. For a fixed value of u* equation (7) shows that the flow velocity u_1 increases as the specific potential energy w becomes larger. Thus we have inequality (8).

$$u_1 > u^* \tag{8}$$

Under certain conditions w might be so large that the difference between u_1 and U would be undetectable. Formal substitution shows u_1 is as large as U when w is as large as $u_1^2/2 + 3c_0^2/2$. Table I for argon initially at room temperature and a pressure of 1 mm Hg was constructed from the graphs given by Resler, Lin, and Kantrowitz.[26] The table shows how the per cent of difference between the shock velocity U and the flow velocity u_1 decreases as w the potential energy in the form of ionization increases. In this table α is the number of positive argon ions per unit volume divided by the number of argon nuclei per unit volume. If the shock had produced no ionization , equation (8) could have been used to

show that the percent of difference between U and u_1 would have approached 28.57··· per cent as the shock velocity U increased. It should be noted that equation (2) indicates that the per cent of difference can never become zero, since u_1=U implies infinite compression by the shock.

TABLE I

PERCENT OF DIFFERENCE BETWEEN U AND u_1 FOR SHOCKS IN ARGON

Mach Number of Shock	α= Mole Fraction of Shock Produced Ions	Percent of Difference Between U and u_1
10	.01	27
12	.035	22
14	.09	17
16	.14	16
18	.21	13

CHAPTER IV

DESCRIPTION OF EQUIPMENT

The construction of the discharge tube is shown in figure 1. The polarity of the electrodes was found to affect only the initial phases of the discharge even though the expansion avenue was unsymetrically located with respect to the two electrodes. The electrodes were of brass machined to make a smooth inner surface to the discharge tube, for it has been found that minute surface irregularities can disturb the velocity field.

The discharge tube was sealed to a glass vacuum system consisting of an oil diffusion pump, a McLeod pressure gauge, and flasks of helium, neon, argon, and xenon. Pressure-adjusting stopcocks permitted the introduction of various amounts of these gases into the previously evacuated discharge tube. All these gases were available spectrographically pure; however, He pressures of 29.5 and 91 mm of Hg were obtained by using gas from a cylinder of grade "A" He.

In all the quantitative experiments electrical energy was supplied to the tube by the damped discharge of a 16.65 μfd capacitor through a circuit consisting of a solenoid operated vacuum switch, the tube, a current measuring

non-inductive resistance, a single turn loop used for triggering a syncroscope sweep, and two damping resistors incorporated in a resistance input π-section filter with .1 μfd capacitors. The 16.65 μfd capacitor was charged to potentials up to 5000 volts by a power supplying circuit that was disconnected before each discharge occurred. The entire charging and discharging circuits were shielded from the electrical circuits used in studying the discharge according to the technique described by Clotfelter.[29] The capacitor potential was estimated to be known with an accuracy better than $\pm$ 7%.

The time and position variation of light output during the discharge were studied by using a rotating concave mirror to image the length of the tube on a stationary photographic film. A synchronizing electro-optical system was used to initiate the discharge at the proper instant to insure the recording of the tube image on the photographic film. The mirror speed of 28.6 rps was measured by a binary scaler with pulse counter and also by a tachometer. From the mirrorgrams produced by this wave speed camera the velocity u of the advancing luminosity could be found quite readily by using equation (9).

$$u = 27.3 \times 10^4 \tan\phi, \text{ cm /sec}, \tag{9}$$

where 27.3×10^4 is a numerical factor found from mirror speed, image distance of 115.1 cm, and object distance of 759 cm, and ϕ is the angle between time axis of mirrorgram

and front whose velocity is to be found. This mirror system has been described more fully by Lee and Fowler.[8]

A Tektronix 514-D cathode-ray oscilloscope was used to study many of the transient characteristics of the discharge. The National Bureau of Standards radio station WWV was used to adjust a 100 kilocycle crystal-controlled secondary standard that modulated the intensity of the electron beam striking the oscilloscope screen. Usually the sweep was initiated by the voltage pulse induced in a small one-turn coil wound adjacent to a similar coil mentioned earlier as being included in the discharge circuit. By displaying on the Y axis a signal proportional to the current through the discharge tube, the method of initiating the sweep was found to be reproducible with time deviations from the mean being less than ± 0.25 sec.

Standard photographic techniques were used in developing both the oscillograms and the mirrorgrams. A combined measuring microscope and microprotractor was then used to determine angles and positions recorded on the films. Angle measurements were reproducible to ± 0.1 degree for the best quality mirrorgrams while distances of 10 mm were often reproducible to ± 0.1 mm. The photographic reproductions of the oscilloscope trace contained a distortion due to curvature of the cathode ray tube screen. Most of this error was compensated for by the technique used in calibrating sweep speeds, so that the error introduced here was less than $\pm 7\%$.

In as much as the non-luminous shocks were purely hypothetical in the early stages of this research, a few pages will be used in describing shock detectors and their limitations. Nearly any colligative property of a gas such as its index of refraction, temperature, pressure, electrical conductivity, or density is discontinuous across the shock and might be used as a basis of a shock detector; thus an almost unlimited number of devices seem suitable. There are, however, restrictive requirements which any detector for shocks in the discharge tube should satisfy. First of all, the device should have a response time not much greater than a microsecond for shocks in low density gases. Secondly, the device should not stop functioning after being exposed to conductors carrying currents that rise to 5000 amperes in less than 5 microseconds. Last of all, the device should be effective in presence of a photon flux as intense as that produced in the interior of a photoflash bulb. The last requirement prevents the use of standard shadowgraph, schlieren, and interferometric techniques in which no provision is made to shield the photographic plate from the light which subsequently originates from the position where the shock was to have been detected. Experience with the rotating mirror also discouraged attempts to shield the recording film from this later undesirable light by directing the light away from that portion of the film exposed by the shock's passage. The low particle densities

also rendered dubious the use of these optical methods.

Many experiments were made in which a glow discharge served as a detector. The shock, in passing over a small glow discharge, changed the discharge current and also the light output; thus shock arrival times could easily be obtained, and there was even some hope that such a discharge might be calibrated to indicate the density behind the shock. The simplest detector built on these principles consisted of two needle-like electrodes introduced through opposite sides of the discharge tube. Current changes in the 1 mm long glow discharge between the tips of these electrodes were converted by a load resistor into voltage changes, which were applied to the vertical plates of an oscilloscope triggered by the discharge of the 16.65 μfd capacitor supplying energy to the shock tube. The response time was excellent, but this feature was offset by many undesirable effects. Photons from the main discharge apparently changed the operating characteristics of the detecting glow discharge either by photoionization of the gas or by photoelectric effect on the electrodes. Whatever the origin of the undesired signal was, it invariably arrived at the detector with no measurable time lag. At times, this early signal was so severe that the shock's passage at some later time was not detectable. Another shortcoming of this device was that for certain shock strengths and initial specific volumes the detector's current was increased while for other strengths and specific

volumes the current was decreased. By placing the detecting gap at various radial distances from the center of the tube, the arrival time of the center of the shock was found to be within a microsecond of the arrival of the outer edge of the shock front. Further analysis of this device seems desirable, since it may yield unique and valuable knowledge of the expansion.

An electrodeless discharge was also used as a detector. This discharge was excited by a tuned-grid tuned-plate self-biasing pushpull oscillator designed to be very unstable. The grid bias developed by the circuit depended upon the amount of energy being delivered by the oscillator to the discharge inside the shock tube.. This energy depended in turn on properties of the gas which were changed by the shock's passage. The shock was often found to produce an easily detectable 50 volt change in grid bias. The device had two advantages over other detectors arising from the fact that it was completely external to the discharge tube. The first of these was the ease with which the detector could be moved to various positions along the expansion chamber. Secondly, the device did not disrupt the flow; consequently the shock could pass through the sensitive region, be reflected by an obstruction, and then be recorded upon passing back through the sensitive region. Altogether four oscillators, ranging in frequency from 10 to 300 megacycles, were constructed in an attempt to reduce the length

of the sensitive region by confining the RF field to a smaller volume inside the shock tube. In addition, variously shaped conductors were placed in positions required by Lenz's law to reduce the volume of the sensitive region. These efforts were not very successful. Other discouraging factors included the defects common to the glow discharge with electrodes; namely, the discharge was photon sensitive, and also the signal polarity depended on shock strength and initial specific volume.

Some experiments were also performed to see how well phototubes could supplement or even replace the wave speed camera used for obtaining luminous front velocities. The expected shock or luminous front signal was nearly always masked by an earlier signal thought to be caused by light scattered from the glass walls, fluorescence of the walls, or photoexcitation of the gas. This early signal could be partially eliminated by using two photocells in a difference circuit in which the subtrahend photocell was focused on the wall alone, while the minuend photocell was set to receive the signal from the gas as well as the signal from the glass. Studies with filters and also a monochrometer indicated that a wave length discrimination of the early undesirable signal and the later signal was possible. The fact that the early signal was associated with the longer wave lengths favors fluorescence of the walls as the cause of the early signal. In experiments with a photomultiplier the large currents of 5000 amperes were found to produce magnetic fields that

disturbed the electron paths within the photomultiplier and thus to produce another undesirable signal.

A piezoelectric crystal was also tried as a shock detector with very crude apparatus. The crystal required a high gain amplifier to detect the feeble signal generated by the shocks in the low density gas. Shielding problems discouraged a thorough investigation of this detector's potentialities.

The most satisfactory detector was found to be a simple low impedance 40 ohm magnetic earphone converted into a low response time shock detector by replacing the diaphragm with 0.002 inch iron shim stock. This detector was placed in the tube so that its diaphragm completely obstructed any flow by filling the entire tube cross section. The earphone was connected by a nylon cord to an iron counter weight whose position could be changed with an exterior solenoid even though the counter weight itself was inside the vacuum system. With this arrangement, the detector's position was known or could be set to the nearest millimeter. A flexible shielded wire connected the movable detector to terminals leading outside of the discharge tube. As might be expected, objectional vapors were given off by parts of this detector; and nearly a month of constant pumping was needed to eliminate them. This shock transducer gave about a five volt signal that was registered by the camera of the oscilloscope. Multiple exposures with the camera could be

distinguished from single exposures by their blackness alone, thus the reproducibility of transit time was better than $\pm .5$ microsecond. Even this detector, completely shielded as it was, gave an unwanted but distinguishable early signal, probably caused by a combination of photoelectric and electromagnetic induction effects. The magnetic transducer was also used to produce a stopping signal for turning off a binary counter chronometer. The abrupt rise in discharge tube current was used to start the counter registering the number of positive pulses generated by a one megacycle crystal-controlled oscillator. Thus by simply reading the number registered by the counter, one could obtain directly the number of microseconds required for the shock to reach the position of the detector. Pairs of these arrival times had an average per cent of difference less than 7%. A functional diagram of the counter chronometer is given in figure 2. Shock velocities found with this transducer agreed with the mirrorgram velocities of luminous fronts that had been qualitatively identified as shocks.

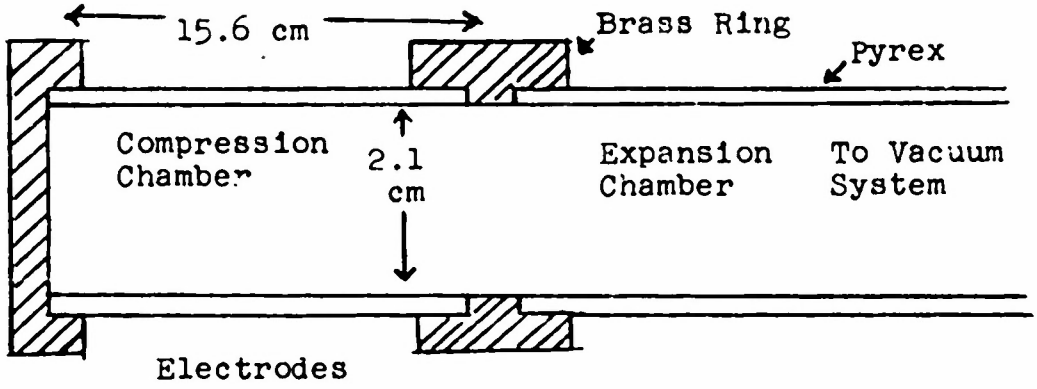

Figure 1 Discharge Tube

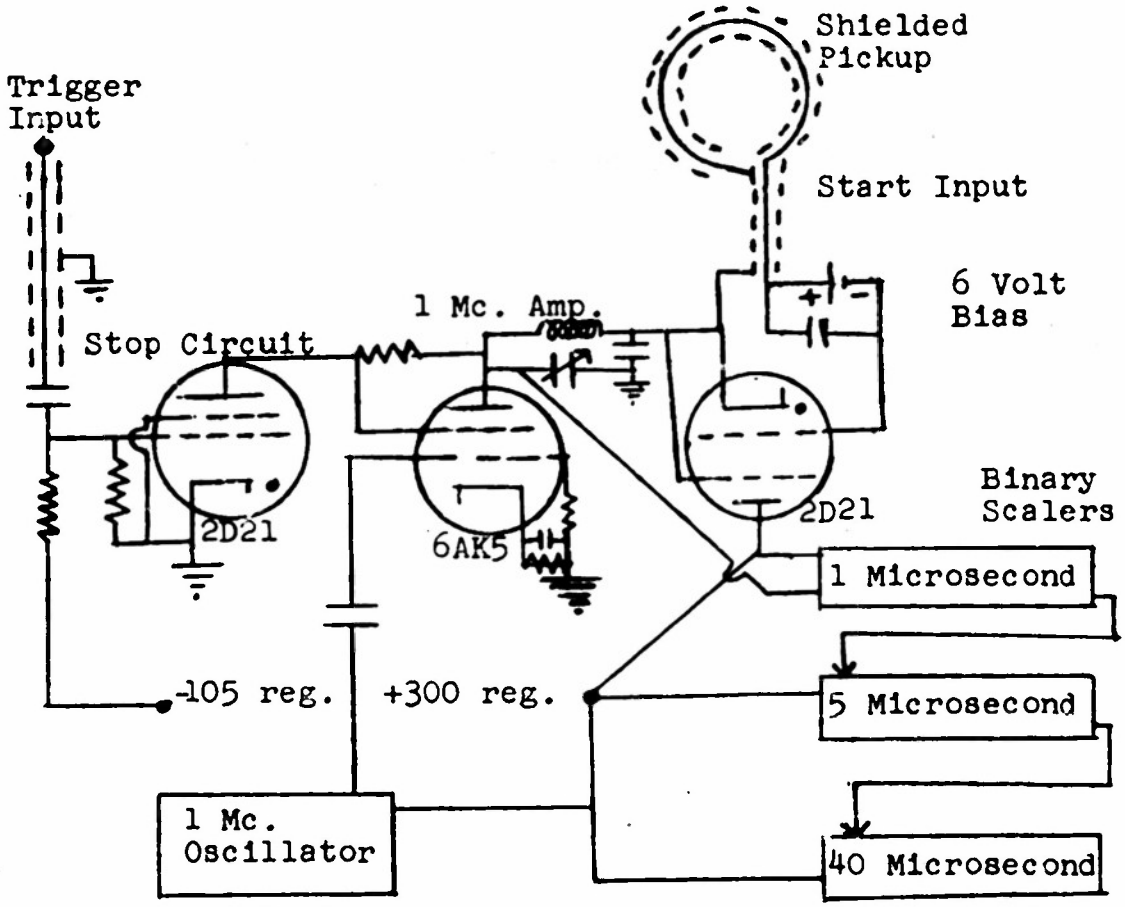

Figure 2 Counter Chronometer

CHAPTER V

MEASUREMENTS

Throughout the tables of data, positions along the expansion chamber are measured from the electrode separating the compression chamber and the expansion chamber. The time origin is much more arbitrary and varies from table to table, from one initial pressure to another, and from one discharge potential to another. Even though the time origin is somewhat arbitrary, information about the constancy of shock velocity U and luminous front velocity u is still obtainable from Tables II, III, IV, and V. In some cases, notably helium pressures of 9.3 and 1.6 mm Hg, a deceleration of the shock fronts is detectable, but usually experimental error, arising in part from the uncertainty of shock detector position, masks any systematic deviation of the shock from constant velocity. Over the most linear 12-cm-long regions of time and distance plots constructed from these tables, the scatter of data points is, on the average, small enough to enable the detection of shock attenuations greater than 3×10^{-5} km/sec per μsec for xenon and 6×10^{-4} km/sec per μsec for helium.

Information about the constancy of the luminous front

velocity can best be obtained from Tables XI, XII, XIII, XIV, and XV, which give directly the velocity in kilometers per second at various positions along the expansion chamber. Over the range of experimental conditions studied, the luminous front velocity u decreased on the average to 3/4 of its initial value in a distance of 10 cm. Over certain intervals the velocity u, in a few cases, seemed to increase slightly with distance traveled by the front.

Tables II and IV, which give distance traveled by the shocks as a function of time, were obtained by using the magnetic shock transducer and the calibrated sweep of the oscilloscope to measure the recorded shock arrival times. These times are essentially the time intervals between the initiation of the oscilloscope sweep and the arrival of the shock at the detector. Discharge potential and initial gas pressure affected the build up of current in the discharge tube; consequently the time interval between the triggering of the sweep and the instant of maximum current varied as initial conditions changed. For the above reason no special effort was made to keep the voltage sensitivity of the trigger amplifier constant as initial conditions were changed. In fact, at each new pressure and potential an effort was often made to reduce the sensitivity of the trigger amplifier to a minimum consistent with reproducible triggering. It was through this technique that the arbitrariness in time origin arose; nevertheless, the tables were used to obtain essential

information about shock velocities and their constancy.

Table VI, which also gives distance traveled by a shock as a function of time, was obtained by using the counter chronometer. For the neon pressure of 155.5 mm Hg positions were recorded to the nearest quarter centimeter. The times indicated in Table V are essentially the time intervals between the triggering of the chronometer and the arrival of the shock at the magnetic transducer. The triggering was accomplished by using the voltage generated in a small loop placed close to the discharge circuit. No special effort was made to place this loop in the same position for the two sections of Table V; so that a certain arbitrariness in time origin occurs again. For the neon pressure of 155.5 mm Hg a shock velocity of 0.90 km/sec found with the chronometer compares with a value of 0.93 km/sec obtained by timing techniques using the oscilloscope.

Tables III and V, which give distances traveled by the luminous fronts as functions of time, were obtained from the mirrorgrams by using the measuring microscope to measure distances. For the one case of xenon at a pressure of 1.6 mm Hg in Table III, a special effort was made to choose a time origin coincident with the time origin used in the first section of Table I. The time origins used in the other sections of Tables III and V are evident from inspection of the tables.

The shock velocities in Tables VII and VIII came in

part from Tables II and IV respectively. The rest of the shock velocities in Tables VII and VIII as well as all of the velocities in Tables XIV and X were obtained by taking additional measurements with the shock transducer and the oscilloscope. The method used in taking these measurements was to find the shock arrival time at the two positions indicated in the range column of the tables. Usually two or three measurements were made of each arrival time. Thus each velocity in these tables is an average over several trials as well as an average over an approximate 10 cm interval.

Tables XII, XIII, XIV, and XV are the main tables. Since the luminous front velocity was not too constant throughout the expansion, the velocity was usually determined at several positions along the expansion chamber. Equation (9) was ordinarily used to obtain these velocities, but in some cases the velocities were obtained from Tables III and V. The velocities obtained from Tables III and V were not velocities at a particular position but rather the average velocities over certain intervals. The position or range of positions corresponding to each velocity determination is indicated by a column heading or by parenthesis. In Table X all but two of the velocities listed for helium pressures of 15.3 and 7.6 mm Hg were obtained by interpolation of velocity measurements given in Table XI. This interpolation tended to smooth the data and eliminate wild

measurements. Graphical interpolation processes were applied to nearly all the data in Tables VIII, VII, IX, and X, in order to obtain the shock velocities at discharge potentials for which the luminous front velocities were known. From these smoothed-out or interpolated shock velocities, the flow velocities u*, given by equation (6) were calculated. The average room temperature of 33° C was used in computing the sound speed substituted into equation (6). These flow velocities are listed in Tables XII, XIII, XIV, and XV.

TABLE II

TIME AND POSITION RELATIONSHIPS FOR XENON SHOCKS

Time μsec		Position cm
50		5.8
61		6.9
70		8.0
83		9.1
98		10.6
104		11.5
136		14.0
150		15.2
160	Pressure 1.6 mm of Hg	16.3
180		17.4
190	Potential 4780 volts	18.8
210		19.9
270		23.3
350		28.0
430		32.7
500		36.3
560		40.2
780		50.4
810		51.0
860		53.3
920		55.7
1020		59.1
1130		63.1
1200		66.0
1260		68.0
1300		69.9
34		2.1
44		3.0
48		3.4
53		4.2
58		4.6
74	Pressure 2.9 mm of Hg	5.8
89		7.0
106	Potential 3000 volts	8.2
122		9.3
132		10.3
150		11.7
170		12.8
190		14.2
200		15.1
210		16.4

TABLE II--Continued

Time μsec		Position cm
240		17.5
250		18.6
270		20.0
43		2.1
56		3.1
75		4.4
97		5.7
114		6.8
136		8.3
150		9.1
170	Pressure 9.2 mm of Hg	10.3
200		11.8
210	Potential 3020 volts	12.8
230		13.8
250		15.4
270		16.5
290		17.8
310		18.7
340		20.4
36		2.0
49		3.1
55		3.5
67		4.4
86		5.8
104		7.0
122		8.2
135	Pressure 5.5 mm of Hg	9.1
150		10.3
174	Potential 3020 volts	11.7
186		12.6
210		14.0
220		15.0
250		16.6
270		17.6
290		18.8
310		20.0
65		3.2
90	Pressure 13.7 mm of Hg	4.5
132		6.9
180	Potential 3020 volts	9.2

TABLE II--Continued

Time μsec		Position cm
220		11.7
270		14.4
300		16.2
370		19.1
53		2.0
73		3.1
97		4.5
140		6.9
118		5.7
180		8.0
190	Pressure 19.5 mm of Hg	9.1
210		10.5
230	Potential 3020 volts	11.6
260		12.9
290		14.3
300		15.2
320		16.3
370		18.0
380		18.9
390		20.0

TABLE III

TIME AND POSITION RELATIONSHIPS FOR LUMINOUS FRONTS IN XENON

Time μsec		Position cm
17		2.0
21		2.5
30		3.2
37		3.7
44		4.2
45	Pressure 1.6 mm Hg	4.2
55		4.9
54		4.9
63	Potential 4630 volts	5.3
64		5.4
73		6.0
83		6.5
92		7.1
104		7.6
123		8.6
0.0		1.6
12.0		2.4
21.0		2.8
34		3.7
41	Pressure 2.9 mm Hg	4.0
56		4.8
64	Potential 3020 volts	5.4
78		6.1
86		6.6
98		7.3
0.0		1.6
14.2		2.5
25		2.8
40		3.7
46		4.1
62	Pressure 5.5 mm Hg	4.8
73		5.3
88	Potential 3020 volts	6.1
97		6.5
112		7.2
123		7.7
138		8.5
150		8.8
160		9.6
180		10.1

TABLE III--Continued

Time μsec		Position cm
0.0		1.6
15		2.5
23		2.8
44		3.7
55		4.1
72		4.8
83	Pressure 9.2 mm Hg	5.3
99		6.1
109	Potential 3020 volts	6.5
126		7.2
139		7.7
160		8.5
170		8.8
190		9.6
210		10.1
220		10.8
0.0		7.7
18	Pressure 15.7 mm Hg	8.5
31		8.8
52	Potential 3020 volts	9.6
72		10.1
89		10.8
0.0		1.6
25		2.5
45		2.8
65		3.7
77		4.1
99	Pressure 19.5 mm Hg	4.8
118		5.3
139	Potential 3020 volts	6.1
150		6.5
170		7.2
200		7.7
210		8.5
220		8.8

TABLE IV

TIME AND POSITION RELATIONSHIPS FOR HELIUM SHOCKS

Time μsec		Position cm
19		9.2
22	Pressure 1.6 mm Hg	10.4
26		11.6
29	Potential 3020 volts	12.9
33		14.1
13.5	Pressure 1.6 mm Hg	15.3
17		16.5
22	Potential 3020 volts	17.7
25		19.1
25	New Time Origin	19.1
29		20.0
15		5.7
18		6.8
20		8.0
22		9.2
23		10.5
26	Pressure 5.45 mm Hg	11.6
28		12.8
31	Potential 4680 volts	14.1
34		15.3
36		16.4
38		17.5
40		18.8
43		20.1
14		4.4
17		5.6
18		6.7
21		8.0
22		9.3
24	Pressure 9.3 mm Hg	10.5
26		11.6
29	Potential 4680 volts	12.8
32		14.1
35		15.2
38		16.5
40		17.6
43		18.9
43		18.9
45		20.1

TABLE IV--Continued

Time μsec		Position cm
15		4.3
19		5.6
21		6.9
24		8.1
24		9.2
28	Pressure 15.3 mm Hg	10.5
31		11.6
34	Potential 4680 volts	12.8
36		13.9
40		15.4
44		16.6
46		17.6
49		19.0
52		20.3
20		3.2
25		4.2
28		5.6
33		6.6
38		8.0
43		9.1
48	Pressure 28.1 mm Hg	10.5
54		11.7
59	Potential 1570 volts	12.7
64		14.0
70		15.4
75		16.5
79		17.5
84		18.8
91		20.2
17		3.2
20		4.4
25		5.8
28		6.8
34		8.1
37		9.3
41	Pressure 28.1 mm Hg	10.6
46		11.8
50	Potential 3020 volts	12.8
53		14.0
59		15.4
63		16.5
68		17.7
74		19.0
78		20.3

TABLE IV--Continued

Time μsec		Position cm
30		9.2
34		10.6
37		11.6
42	Pressure 28.1 mm Hg	12.8
45		14.1
49	Potential 4680 volts	15.4
52		16.4
57		17.6
61		18.9
65		20.1
18		4.5
25		8.0
39	Pressure 51.3 mm Hg	10.5
47		12.8
56	Potential 4680 volts	15.3
64		17.6
72		20.1
27		5.6
34		8.0
43		10.3
49	Pressure 51.3 mm Hg	11.8
58		14.0
67	Potential 3020 volts	16.4
73		17.6
76		18.9
82		20.1
27		5.7
36		8.0
47	Pressure 61 mm Hg	10.6
56		12.8
66	Potential 3020 volts	15.2
75		17.6
84		20.1
23		5.5
31	Pressure [illegible] mm Hg	8.1
40		10.5
47	Potential 4680 volts	12.8

TABLE IV--Continued

Time μsec	Position cm
58	15.3
67	17.6
75	20.1

TABLE V

TIME AND POSITION RELATIONSHIPS FOR LUMINOUS FRONTS IN HELIUM

Time μsec		Position cm
0.0		1.6
1.7		2.5
4.8		3.7
5.5		4.1
7.2		4.9
8.7	Pressure 1.6 mm Hg	5.3
10.6		6.2
12.0	Potential 3020 volts	6.5
13.7		7.3
16.[illegible]		7.7
17.6		8.5
20.2		8.8
22		9.7
25		10.1
27		10.9
30		11.3
2.6		2.9
0.0		1.6
.7		2.5
1.7		2.8
2.6		3.7
3.4		4.1
4.6		4.8
5.3		5.3
6.3		6.1
7.0		6.5
8.0		7.2
8.9	Pressure 1.6 mm Hg	7.7
9.9		8.5
10.8	Potential 4680 volts	8.8
12.0		9.6
13.2		10.1
14.2		10.8
15.6		11.3
17		12.2
18		12.5
19		13.3
20		13.7
22		14.5
24		15.0
25		15.8

TABLE VI

TIME AND POSITION RELATIONSHIPS FOR NEON SHOCKS

Time μsec		Position cm
96		4.75
123		7.25
129		8.00
152		8.75
141		9.25
158		10.50
177		11.75
179		12.75
186		13.00
197		14.00
194		14.25
193		15.25
220	Pressure 155.5 mm Hg	16.75
223		16.50
228	Potential 3780 volts	17.25
235		17.25
254		18.75
269		20.25
292		23.25
321		25.75
327		26.00
335		28.00
380		30.75
417		33.00
467		38.00
492		40.25
528		45.00
622		47.25
576		50.00
669		56.25
703		58.00
728		59.25
748		61.00
757		61.75
777		62.25

TABLE VI--Continued

Time μsec		Position cm
58		1.8
63		3.8
74		6.6
90		9.1
101		11.6
122		15.2
147		18.8
176		23.2
208	Pressure 7.2 mm Hg	28.1
236		31.6
262	Potential 3460 volts	35.0
303		40.4
342		44.8
386		49.8
440		56.9
507		63.6

TABLE VII

AVERAGE VELOCITIES OF SHOCK FRONTS IN XENON

Pressure mm Hg	Potential volts	Velocity km/sec	Range Over Which Average Was Taken cm
1.6	4630	.93	3 - 7
2.9	3020	.72	4 - 20
5.5	3020	.69	3 - 16
9.2	3020	.61	3 - 20
15.7	3020	.55	3 - 16
19.5	3020	.57	1 - 6
29.5	4830	.58	4 - 13
29.5	4090	.53	4 - 13
29.5	3320	.53	4 - 13
29.5	2570	.50	4 - 13
1.3	4830	.90	6 - 16
1.3	4090	.81	6 - 16
1.3	3320	.78	6 - 16
1.3	2570	.72	6 - 16
1.3	1850	.64	6 - 16
1.3	1140	.53	6 - 16
3.2	4830	.86	4 - 13
3.2	4090	.80	4 - 13
3.2	3320	.77	4 - 13
3.2	2570	.69	4 - 13
3.2	1850	.63	4 - 13

TABLE VIII

AVERAGE VELOCITIES OF SHOCK FRONTS IN HELIUM

Pressure mm Hg	Potential volts	Velocity km/sec	Range Over Which Average Was Taken cm
7.6	706	2.3	10 - 20
7.6	995	2.1	10 - 20
7.6	1420	2.5	10 - 20
7.6	1700	3.0	10 - 20
7.6	2000	3.3	10 - 20
7.6	2420	3.6	10 - 20
7.6	2870	4.3	10 - 20
7.6	3165	4.7	10 - 20
7.6	3460	4.8	10 - 20
7.6	3780	5.1	10 - 20
7.6	4245	5.4	10 - 20
7.6	4525	5.3	10 - 20
7.6	4830	5.7	10 - 20
15.3	1140	2.3	10 - 20
15.3	1710	2.4	10 - 20
15.3	2270	2.6	10 - 20
15.3	2870	2.9	10 - 20
15.3	3460	3.2	10 - 20
15.3	4090	3.5	10 - 20
15.3	4680	4.0	10 - 20
29.5	1140	2.1	10 - 20
29.5	1710	2.6	10 - 20
29.5	2270	3.2	10 - 20
29.5	2870	2.5	10 - 20
29.5	3460	2.6	10 - 20
29.5	4090	3.0	10 - 20
29.5	4680	3.1	10 - 20
91.	2720	2.0	8.5 - 19.5
91.	3170	2.3	6.5 - 19.5
91.	3780	2.4	4 - 20
91.	4390	2.7	4 - 20
91.	4830	2.7	5 - 20
28.1	1567	2.9	5 - 20
28.1	3020	2.7	5 - 20
28.1	4680	3.2	5 - 20
15.3	4680	4.8	1 - 9
15.3	4680	4.1	9 - 18
9.3	4680	6.0	4 - 10
9.3	4680	4.3	10 - 19
5.45	4680	5.2	5 - 19
1.6	4680	6.1	15 - 17

TABLE VIII--Continued

Pressure mm Hg	Potential volts	Velocity km/sec	Range Over Which Average Was Taken cm
1.6	3020	3.1	15 - 18
1.6	3020	3.8	9 - 13
61.	3020	2.5	5 - 20
61.	4680	2.7	5 - 20
51.3	3020	2.6	5 - 20
51.3	4680	2.9	4 - 20

TABLE IX

AVERAGE VELOCITIES OF SHOCK FRONTS IN NEON

Pressure mm Hg	Potential volts	Velocity km/sec	Range Over Which Average Was Taken cm
.94	4390	3.0	10 - 13
.94	3620	1.5	12 - 20
.94	2870	1.3	11 - 20
.94	2130	1.1	12 - 20
2.0	4680	2.1	7 - 20
2.0	4090	1.8	10 - 20
2.0	3460	1.5	7 - 19
2.0	2870	1.4	8 - 20
2.0	2270	1.3	8 - 19
5.35	4680	1.8	6 - 20
5.35	4090	1.7	6 - 20
5.35	3460	1.6	6 - 20
5.35	2870	1.5	6 - 20
5.35	2270	1.3	6 - 20
5.35	1710	1.2	5 - 20
5.35	1140	1.1	5 - 20
8.3	4830	1.9	5 - 20
8.3	4390	1.8	6 - 20
8.3	3780	1.6	6 - 20
8.3	3170	1.6	6 - 20
8.3	2570	1.3	6 - 20
8.3	1990	1.2	6 - 20
12	4830	1.9	6 - 20
12	4390	1.6	6 - 20
12	3780	1.5	6 - 20
12	3170	1.3	6 - 20
12	2570	1.2	6 - 20
12	1990	1.1	6 - 20
17.7	4980	1.6	6 - 20
17.7	4390	1.5	6 - 20
17.7	3620	1.3	6 - 20
17.7	2870	1.2	6 - 20
17.7	2130	1.1	6 - 20
17.7	1420	.99	6 - 20
27.6	4830	1.4	6 - 20
27.6	4090	1.28	6 - 20
27.6	3320	1.17	6 - 20
27.6	2570	1.09	6 - 20
27.6	1850	1.00	6 - 19
52	4830	1.24	4 - 12
52	4090	1.16	3 - 12
52	3320	1.11	3 - 12

TABLE IX--Continued

Pressure mm Hg	Potential volts	Velocity km/sec	Range Over Which Average Was Taken cm
52	2570	1.05	3 - 12
52	1850	1.00	3 - 12
92.5	4980	1.14	4 - 13
92.5	4240	1.08	4 - 13
92.5	3460	1.02	4 - 13
92.5	2720	.96	4 - 13
92.5	1990	.89	4 - 13
92.5	1420	.82	4 - 13
155.5	4980	1.02	4 - 13
155.5	4240	.97	4 - 13
155.5	3460	.91	4 - 14
155.5	2720	.87	4 - 14
155.5	1990	.77	4 - 14

TABLE X

AVERAGE VELOCITIES OF SHOCK FRONTS IN ARGON

Pressure mm Hg	Potential volts	Velocity km/sec	Range Over Which Average Was Taken cm
1.15	4830	1.7	9 - 19
1.15	4090	1.6	9 - 19
1.15	3320	1.4	9 - 19
1.15	2570	1.25	9 - 19
1.15	1710	.99	9 - 19
3.1	4830	1.6	9 - 19
3.1	4090	1.5	9 - 19
3.1	3320	1.3	9 - 19
3.1	2570	1.16	9 - 19
3.1	1850	1.01	9 - 19
8.7	4830	1.21	9 - 20
8.7	4090	1.19	9 - 20
8.7	3320	1.07	9 - 20
8.7	2570	.99	9 - 20
8.7	1850	.88	9 - 20
8.7	1140	.86	9 - 20
8.7	850	.77	9 - 20
28.4	4830	1.07	9 - 20
28.4	4090	1.02	9 - 20
28.4	3320	.95	9 - 20
28.4	2570	.88	9 - 20
28.4	1850	.78	9 - 20

TABLE XI

LUMINOUS FRONT VELOCITIES IN HELIUM

Pressure mm of Hg	Potential in volts	Velocity in km/sec at Position 4.1 cm	8.8 cm	13.7 cm
15.3	4800	4.0	3.2	2.5
15.3	4220	3.6	2.6	2.3
15.3	3680	3.2	2.2	2.2
15.3	3050	2.6	2.1	2.0
15.3	2450	2.3	1.9	1.7
15.3	1850	2.1	1.7	1.5
15.3	1240	1.9	1.3	
		5.3 cm		14.9 cm
7.6	4740	4.5		2.7
7.6	4380	4.2		2.6
7.6	4000	4.1		2.5
7.6	3660	3.9		2.4
7.6	3340	3.7		2.3
7.6	3010	3.5		2.2
7.6	2630	3.2		2.0
7.6	2240	2.8		1.9
7.6	1910	2.2		1.5
7.6	1540	2.2		1.6

TABLE XII

LUMINOUS FRONT VELOCITIES u AND FLOW VELOCITIES u* IN HELIUM

Numbers in parenthesis beside the velocity u indicate either the position in cm at which measurement was made or the position range in cm over which average velocity was determined.

Pressure mm Hg	Potential volts	u km/sec			u* km/sec
28.1	4680	2.8 (1.6-5.3)	2.2(10.1-11.5)		2.2
28.1	3020	2.1 (8.8)			1.8
28.1	1570	1.4 (3-11.5)			1.4
15.3	4680	3.6 (1.5-9.5)			3.4
15.3	4680	2.4 (9.5-18.5)			2.9
15.3	1420	2.0 (4.1)	1.4(8.8)		1.5
15.3	1710	2.1 (4.1)	1.6(8.8)		1.6
15.3	1990	2.2 (4.1)	1.7(8.8)	1.5(13.7)	1.6
15.3	2270	2.2 (4.1)	1.8(8.8)	1.6(13.7)	1.7
15.3	2570	2.3 (4.1)	1.9(8.8)	1.8(13.7)	1.8
15.3	2870	2.5 (4.1)	2.0(8.8)	1.9(13.7)	1.9
15.3	3170	2.6 (4.1)	2.1(8.8)	2.0(13.7)	2.1
15.3	3460	2.7 (4.1)	2.2(8.8)	2.1(13.7)	2.2
15.3	3780	2.9 (4.1)	2.3(8.8)	2.2(13.7)	2.3
15.3	4090	3.4 (4.1)	2.5(8.8)	2.3(13.7)	2.5
15.3	4390	3.7 (4.1)	2.8(8.8)	2.4(13.7)	2.7
15.3	4680	3.9 (4.1)	3.0(8.8)	2.5(13.7)	2.9
9.3	4680	4.5 (4.5-10.5)			4.5
9.3	4680	2.5 (6.5-14.5)			3.0
5.45	4680	5.0 (1.5-6.5)			3.7
1.6	4680	6.4 (2.5-6.5)	3.8(10.5-14.5)		4.4
1.6	3020	2.4 (7.5-10.5)			3.0
1.6	3020	4.0 (1.5-6.5)			3.8
7.6	565	1.5 (5.3)	1.1(14.9)		1.0
7.6	850	1.8 (5.3)	1.2(14.9)		1.3
7.6	1140	2.0 (5.3)	1.3(14.9)		1.5
7.6	1420	2.2 (5.3)	1.5(14.9)		1.8
7.6	1710	2.4 (5.3)	1.6(14.9)		2.0
7.6	1990	2.6 (5.3)	1.7(14.9)		2.2
7.6	2270	2.8 (5.3)	1.9(14.9)		2.5
7.6	2570	3.1 (5.3)	2.0(14.9)		2.7
7.6	2870	3.3 (5.3)	2.1(14.9)		2.9
7.6	3170	3.5 (5.3)	2.2(14.9)		3.1
7.6	3460	3.7 (5.3)	2.3(14.9)		3.3
7.6	3780	3.9 (5.3)	2.4(14.9)		3.5

TABLE XII--Continued

Pressure mm Hg	Potential volts		u km/sec		u* km/sec
7.6	4090	4.1 (5.3)	2.5(14.9)		3.8
7.6	4390	4.3 (5.3)	2.6(14.9)		4.0
7.6	4680	4.6 (5.3)	2.7(14.9)		4.2
7.6	4980	4.8 (5.3)	2.7(14.9)		4.4
29.5	4680	2.8 (4.1)	2.4(8.8)	2.1(13.7)	2.1
29.5	4180	2.4 (4.1)	2.2(8.8)	2.0(13.7)	2.0
29.5	3670	2.0 (4.1)	2.2(8.8)	2.0(13.7)	1.9
29.5	3060	1.8 (4.1)	2.1(8.8)	1.7(13.7)	1.7
29.5	2450	1.6 (4.1)	2.0(8.8)	1.5(13.7)	1.5
29.5	1860	1.6 (4.1)	1.7(8.8)	1.3(13.7)	1.4
29.5	1250	1.6 (4.1)	1.6(8.8)		1.2
51.3	3020	1.4 (15)			1.6
51.3	4680	1.6 (16.2)			1.9
61	3020	1.2 (15)			1.6
61	4680	1.6 (16.2)			1.8
91	4950	1.8 (4.1)	1.8(8.8)	1.7(13.7)	1.8
91	4390	1.8 (4.1)	1.9(8.8)	1.4(13.7)	1.7
91	3810	1.5 (4.1)	1.5(8.8)	1.3(13.7)	1.5
91	3160	1.4 (4.1)	1.5(8.8)	1.0(13.7)	1.4
91	2510	1.2 (4.1)	1.2(8.8)	.9(13.7)	.9

TABLE XIII

LUMINOUS FRONT VELOCITIES u AND FLOW VELOCITIES u* IN XENON

Numbers in parenthesis beside the velocity u indicate either the position in cm at which measurement was made or the position range in cm over which average velocity was determined.

Pressure mm Hg	Potential volts	u km/sec				u* km/sec
19.5	3020	.33	(1.5-8.5)			.38
15.7	3020	.32	(8.5-11.5)			.37
9.2	3020	.43	(2.5-7.5			.42
5.5	3020	.48	(1.5-9.5)			.48
2.9	3020	.57	(1.5-7.5)			.51
1.6	4630	.60	(3.5-8.5)			.68
3.2	4840	.67	(4.1)			.61
3.2	4300	.57	(4.1)			.59
3.2	3750	.61	(4.1)			.56
3.2	3070	.56	(4.1)			.53
3.2	2450	.56	(4.1)			.48
3.2	1850	.45	(4.1)			.42
1.3	4820	.88	(4.1)			.64
1.3	4270	.72	(4.1)			.60
1.3	3650	.71	(4.1)			.57
1.3	3050	.67	(4.1)			.53
1.3	2450	.66	(4.1)			.49
1.3	1850	.57	(4.1)			.44
1.3	1220	.47	(4.1)			.36
29.5	4950	.51	(4.1)	.53	(8.8)	.40
29.5	4450	.40	(4.1)	.43	(8.8)	.37
29.5	3840	.38	(4.1)	.32	(8.8)	.36
29.5	3160	.39	(4.1)	.32	(8.8)	.35
29.5	2540	.33	(4.1)	.32	(8.8)	.33

TABLE XIV
LUMINOUS FRONT VELOCITIES u AND FLOW VELOCITIES u* IN NEON

Pressure mm Hg	Potential volts	u in km /sec at 4.1 cm	8.8 cm	13.7 cm	u* in km /sec
.94	4330	3.1	1.7		1.2
.94	3780	2.8	1.5		1.1
.94	3140	2.3	1.0		.93
.94	2520	1.7			.76
.94	1910	1.5			.58
2.0	4670		1.5	1.1	1.4
2.0	4270	1.8	1.4	1.0	1.3
2.0	3680	1.7	1.3		1.1
2.0	3050	1.6	1.1		1.0
2.0	2420	1.4			.90
5.35	4920	1.6	1.4	1.2	1.3
5.35	4320	1.5	1.3	1.1	1.2
5.35	3780	1.4	1.2	.92	1.1
5.35	3070	1.3	1.2	.85	1.1
5.35	2520	1.1	1.0		.91
5.35	1880	.91	.83		.75
5.35	1220	.81			.66
8.3	4770	1.5	1.4	1.1	1.3
8.3	4380	1.4	1.3	1.1	1.3
8.3	3780	1.3	1.2		1.1
8.3	3160	1.1	1.0	.81	1.0
8.3	2570	1.0	.75		.86
8.3	1990	.84			.74
12	4890	1.5	1.3	1.1	1.3
12	4370		1.2	1.0	1.2
12	3780	1.1	1.1		1.1
12	3140	.87	.79		.85
12	2490	.87	.72		.73
12	1880	.74	.53		.67
17.7	4950	1.2	1.1	.90	1.1
17.7	4420	1.1	1.1	.78	1.0
17.7	3840	.93	.86		.87
17.7	3160	.87	.70	.72	.79
17.7	2540	.80	.64		.70
17.7	1880	.67	.58		.63
17.7	1250	.72			.59
27.6	4770	1.0	.88	.81	.90
27.6	4330	1.0	.79		.85
27.6	3710	.88	.73		.79
27.6	3080	.83	.75		.73
27.6	2480	.74	.72		.67

TABLE XIV--Continued

Pressure mm Hg	Potential volts	u in km /sec at 4.1 cm	8.8 cm	13.7 cm	u* in km /sec
27.6	1850	.63	.70		.60
52	4780	.90	.88		.80
52	4330	.80	.86		.76
52	3720	.73	.77		.71
52	3140	.67	.75		.67
52	2480	.64	.61		.63
52	1880	.55	.56		.59
92.5	4800	.80	.72		.70
92.5	4090	.71	.63		.66
92.5	3320	.64	.56		.60
92.5	2570	.58	.53		.54
92.5	2130	.53	.48		.49
92.5	1420	.38			.42
155.5	4930	.66	.62		.61
155.5	4380	.68	.63		.58
155.5	3750	.54	.54		.53
155.5	3110	.56	.52		.50
155.5	2500	.43			.45
155.5	1990	.32			.37

TABLE XV

LUMINOUS FRONT VELOCITIES u AND FLOW VELOCITIES u* IN ARGON

Pressure mm Hg	Potential volts	u in km /sec. at 4.1 cm	8.8 cm	13.7 cm	u* in km /sec
1.1	4680	1.9	1.5		1.2
1.1	4090	1.7	1.2	1.1	1.1
1.1	3460	1.5	1.3		1.0
1.1	2860	1.3	1.0		.91
1.1	2270	1.0	1.0		.81
1.1	1710	1.2			.66
3.1	4740	1.5	1.2	.93	1.2
3.1	4270	1.3	1.2	.86	1.1
3.1	3710	1.2	1.1	.86	1.0
3.1	3050	1.2	1.0	.75	.88
3.1	2450	1.0	.89		.78
3.1	1820	.81	.70		.66
8.7	4830	1.05	1.06	.95	.85
8.7	4390	.97	.99	.85	.82
8.7	3780	.82	.93	.71	.77
8.7	3130	.80	.74	.79	.72
8.7	2480	.76	.66		.64
8.7	1880	.76	.65		.57
8.7	1240	.69	.51		.50
8.7	940	.53			.47
28.4	4740	.82	.86	.58	.72
28.4	4330	.75	.76	.62	.70
28.4	3720	.71	.73	.52	.66
28.4	3080	.66	.66	.57	.61
28.4	2520	.69	.56	.61	.56
28.4	1880	.63	.41		.49

CHAPTER VI

INTERPRETATION AND CONCLUSION

Examination of Tables XI, XII, XIII, and XIV shows that gas flow velocities u* are always comparable to the observed luminous front velocities u. In fact, u* is in many cases bracketed by the luminous front velocities found at various positions along the expansion chamber, so that over the range studied, there is little reason to question the identification of the luminous front as the contact surface. A better correlation between the two velocities could not be expected to result from a theory that neglects the deceleration of the fronts. Only when both the shock velocity and the contact surface velocity have remained constant for a time much longer than the transit time of sound between the two fronts, could one expect the flow velocity right behind the shock to agree precisely with the contact surface velocity.

It has been pointed out many times that the simple idealized theory of even the diaphragm shock tube predicts a shock velocity greater than the one found experimentally. This discrepancy, 10% for shock velocities of one km/sec, is often associated with shock velocity determinations being

made before the shock is completely formed.[30] Cassen and Stanton[31] indicate a way by which instantaneous shock velocity measurements may be used to evaluate the spatial derivatives of wake pressure at points adjacent to the shock front. Their work suggests using measured shock attenuations to obtain flow velocities some distance behind the shock front. Section 77 of reference 21 tells of some of the difficulties and uncertainties connected with strong non-uniform shock theory. In addition to the attenuation of the fronts there are two other factors that should be considered before trying to improve the correlation between flow velocities and luminous front velocities. These two factors will be discussed now for they represent an application of the equations of Chapter III.

Suppose that the shock and luminous front velocities are observed to be constant for certain experimental conditions and furthermore suppose that the flow velocity u^* and the luminous front velocity u differ. The problem is then to furnish an explanation. The most obvious explanation would be that the luminous front is not the contact surface; however, there are two explanations consistent with the luminous front being a contact surface. Inequality (8) can be used as an explanation if $u^* < u$ happens to be the case. This would mean that considerable amounts of energy are used in ionizing and exciting the gas atoms as the shock passes over them. If, on the other hand, $u^* > u$ happens to be

the case, then considerable amounts of ionization could be present in the gas even before the shock passes over this region. This last statement follows from an argument patterned after the one used in obtaining inequality (8), and the statement is not at all surprising in view of equation (4), which shows that ionizational augmentation of e_0 should have just the opposite effect of ionizational augmentation of e_1. A mechanism for producing an ionizational augmentation of e_0 can easily be found in the photons produced by the discharge in the compression chamber and there is much qualitative evidence for their importance. These photons would travel through the expansion chamber and could photoionize the gas before the shock arrival. By the time that the shock arrives part of the energy communicated to the gas by the photons could be converted into thermal energy; thus the correct initial sound speed c_0 would not be known. There would be a pre-discharge sound speed c_{00} and a pre-shock sound speed $c_0 > c_{00}$. If c_{00} were used to calculate u*, equation (6) shows that there would again be a tendency to find $u^* > u$.

Probably both of the processes described in the preceeding paragraph, photon preheating and shock produced ionization, are present to some extent in the range of experimental conditions covered by Tables XII, XIII, XIV, and XV. As was pointed out in Chapter II, there are certain experimental conditions for which the <u>shock</u> front is the <u>luminous</u> front, and surely whenever this is the case at least one of

the processes mentioned above is active. Since the two processes have opposite effects on a correlation of u and u*, it is evident that their simultaneous presence could result in a mutual concealment of the presence of either. Because of the attenuation of the luminous front velocity, a rapid survey of the u and u* correlation tables yields little information tending to favor the presence of either of the two processes, unless the attenuation itself is a result of the photon preheating process. Presumably the shock could be traveling into a gas in which photon preheating had established a temperature gradient. If a temperature gradient exists, neither u* nor u would be expected to remain constant.

In Chapter II it was mentioned that under certain experimental conditions the Rayleigh phenomenon exhibits a single luminous front that reaches a piston before reflecting. The identification proposed in Chapter II interpreted the luminous front as a shock being followed by an unobservable contact surface. Some of the results of Chapter III may be used to explain the failure to observe two luminous fronts. This explanation is the one alluded to at the end of Chapter III. As the potential energy contribution to specific internal energy becomes comparable to the specific flow energy, the contact surface velocity and the shock velocity would become less distinguishable. The low initial gas pressures that are necessary for the appearance of the

single luminous fronts which reach the piston, tend to increase both the ionization produced by the shock front and the specific flow energy. If the proposed explanation of these fronts is correct, the specific internal energy in the form of ionization would need to increase more rapidly with decreasing initial pressure than the specific flow energy increases.

In Chapter I it was mentioned that under certain conditions the luminosity produced in the discharge tube appears to move as a slug down the expansion chamber. Many of the mirrorgrams taken at the upper end of the pressure range studied in the data tables had this appearance. Close examination showed that the slug became narrower as it progressed. Now the simple perfect gas theory of shock tube operation indicates that the reflected rarefaction wave would tend to overtake the contact surface; so that the perfect gas theory could explain, through the reflected rarefaction wave, a gradual decrease in temperature behind the contact surface; however, this theory cannot furnish an explanation of abrupt changes in any thermodynamic variable behind the contact surface. Obviously a modification of perfect gas theory is needed just to account for the gas excitation observed behind the contact surface. We shall indicate briefly how the dissociation and recombination required for light production might also account for the luminosity discontinuity behind the contact surface that is

present in the mirrorgrams showing the luminosity advancing as a slug.

Zeldovitch[32] pointed out in 1946 that shock waves of rarefaction are possible under certain conditions in a Van der Waals gas with a large specific heat at constant volume. In 1948 Novikov[33] gave another favorable medium, wet steam in the neighborhood of the critical pressure of approximately 220 atmosphere. Liepmann and Pucket[34] gave a description of moisture condensation shocks. The possibility of shocks of rarefaction in an ionized gas will be considered as an explanation for the mirrorgrams that seem to show a light-quenching front moving through the gas behind the contact surface.

Consider a monatomic gas whose atoms dissociate into B electrons and one positive ion. Here we are mainly concerned with pressure-increasing effects of the dissociation factor so that some other factors and effects, present in all real gases, need not be included. These neglected factors include, among other things, the radiation energy density contribution to internal energy, the radiation pressure, the Coulomb interaction between the ions and electrons, and the presence of atomic particles other than electrons, unexcited atoms, and the unexcited multiply-charged positive ions. The methods of statistical mechanics could be used to treat more realistically the behavior of physical gases which do dissociate into many atomic species. The thermodynamic behavior

of the idealized gas we are considering will be approximated by the following equations.

$$(9)\quad \ln\left[\alpha^{B+1}p^{B}/(1+B\alpha)^{B}(1-\alpha)\right] = -W/kt + (5B\ln T)/2 + C;$$

$$(10)\quad p = (1+B\alpha)kT/m;$$

$$(11)\quad e = 3p\tau/2 + W\alpha/m;$$

where k is Boltzmann's constant,

C is a constant for the gas depending only on the statistical weights of the atom and the ion, and the universal constants,

m is the mass of the neutral atom,

W is the B-degree ionization energy for the atom,

T is absolute temperature,

α is the mole fraction of the ions.

Equation (9) is simply the mass action law coupled with Dalton's law, equation (10) is the perfect gas law corrected for the increased number of particles produced by dissociation, and equation (11) is essentially equation (1).

Using these equations together with $\delta e = -p\delta\tau + T\delta s$ from thermodynamics, one can calculate by implicit partial differentiation $(\partial p/\partial\tau)_s$, $(\partial^2 p/\partial\tau^2)_s$, and $(\partial p/\partial s)_\tau$, the three derivatives that are especially important in shock wave theory. Interestingly enough, the first three shock conditions--equations (2), (3), and (4)--permit both compressive shocks $\tau_0 > \tau_1$ and rarefying shocks $\tau_0 < \tau_1$. Inequality (5) does, however, prohibit one or the other type of shock depending upon the signs of the three previously mentioned

derivatives. For many substances these three derivatives have the same signs as they have for a perfect gas: that is, the first one is negative and the last two are positive throughout the entire p and τ range. When the derivatives have the above signs, rarefying shocks are prohibited by (5). On the other hand, we find for the medium described by equations (9), (10), and (11) that a range of thermodynamic variables exists for which the first two derivatives are negative and the last one positive; consequently upon applying an argument similar to one attributed to Weyl, we find that inequality (5) is satisfied by a shock of rarefaction. Weyl's argument is presented in Courant and Friedrich's book.[21]

It will now be shown that $(\partial^2 p/\partial\tau^2)_s < 0$ establishes a mechanism for the conversion of rarefaction waves into rarefaction shock waves. Let c be the sound speed, we then have the well known formula (12) which may be used to verify (13). The flow velocity u given to a stationary gas at

$$(12) \quad c^2 = -\tau^2(\partial p/\partial \tau)_s$$

$$(13) \quad (-\tau^2/2c)(\partial^2 p/\partial\tau^2)_s = (\partial c/\partial\tau)_s - c/\tau$$

specific volume τ_0 and specific entropy. s_0 by a rarefaction wave is given by the well known equation (14). Using (14) one finds (15) which may be coupled with (13) to yield (16) if $(\partial^2 p/\partial\tau^2)_s < 0$.

$$(14)\quad u = \int_{\tau_0}^{\tau} \frac{c(\tau', s_0)d\tau'}{\tau'}$$

$$(15)\quad (\partial u/\partial \tau)_{s_0,\tau_0} = c/\tau$$

$$(16)\quad [\partial(c-u)/\partial \tau]_s > 0$$

Now c-u is the upstream propagation velocity of small pressure differences and (16) shows this velocity to be greater in the expanded state at the foot of the wave than in the unexpanded state at the head of the rarefaction wave; consequently the rarefaction wave will tend to become steeper. In this manner shocks of rarefaction will form in the medium.

In the discharge tube one could expect a rarefaction wave to move through the compression chamber and reflect from the electrode forming the end of the chamber. The mirrograms show these expected reflections in only a few cases; however, no extensive search for them has been made. If the reflected rarefaction wave travels through a proper medium it would steepen into a rarefaction shock that would probably make the luminosity appear to move as a slug down the expansion chamber. At the present time the theory is believed to be unsatisfactory since all calculations based on equations (9), (10), and (11) have indicated that pressures lower than 10^{-31} dynes/cm^2 are needed in order to have conditions favorable for the shocks of rarefaction. Perhaps a theory that included the possibility of forming atomic complexes would result in a more reasonable pressure range suitable for shocks of rarefaction. The constant entropy approximation could also be improved.

CHAPTER VII

SUMMARY

A shock tube has been constructed in which the pressure difference is created by heating the compression chamber gas with a spark produced by the discharge of a capacitor capable of delivering to the gas about 0.2 joules /cm^3 in a time less than 20 μsec. A rotating-mirror camera was used to study the subsequent motion of helium, neon, argon, and xenon luminosity in the expansion chamber.

Under a wide range of experimental conditions the qualitative appearance of the mirrorgrams corresponded quite well with the flow patterns produced by a diaphragm shock tube. More specifically, it was possible to classify the observed fronts into two categories: C-type luminous fronts which reflect before reaching a piston placed in the expansion chamber, and S-type luminous fronts which reach the piston before reflecting. For certain initial pressures and capacitor potentials the mirrorgrams showed only a brilliant C-type front that might be interpreted as the contact surface; whereas for other conditions the C-type front was preceded by a fainter S-type front travelling with a greater velocity. This S-type front might be interpreted as a luminous shock front.

A shock detector placed in the expansion chamber permitted the determination of the average shock velocity U over an approximate 10 cm interval. The world lines of the shock front and the S-type front coincided. From the shock velocities U an average gas flow velocity u* was computed. During the early stages of the expansion the velocity u* was usually found to be slightly less than the luminous C-type front velocity u. During the later phases of the expansion, u* was usually slightly greater than u. This agreement furnished quantitative evidence that the C-type luminous front had been correctly identified as a contact surface.

As the initial pressure is reduced, the S-type front becomes more and more conspicuous. At pressures less than one mm of Hg it is sometimes impossible to detect a C-type front at all. Ionization by the shock was proposed as an explanation for this low pressure behavior.

In the upper range of initial pressures studied, the luminosity about a cm behind the contact surface was observed to decrease almost discontinuously to a very low value. The simple perfect gas theory of shock tube operation would explain a gradual reduction of light output behind the contact surface, but it fails to explain the discontinuity which suggests a light-quenching wave moving through the tube with a velocity slightly greater than the contact surface velocity. Shock waves of rarefaction are known to be

possible in condensable gases. Theoretical considerations showed that conditions favoring the conversion of rarefaction waves into rarefaction shocks also exist in an ionized gas obeying Saha's equation. Presumably the rarefaction wave reflected from the end of the compression chamber could steepen into a shock of rarefaction and thus account for the abrupt decrease of brilliance behind the contact surface.

BIBLIOGRAPHY

1. A. Toepler, Ann. Phys. Lpz., 131, 33, (1867).

2. E. Mach, Sitzungsber. d. k. Akad. d. Wissensch. zu Wien, 98, 1333, (1889).

3. V. Dvorak, Ann. Phys. Lpz., 9, 502, (1880).

4. M. Toepler, Ann. Phys. Lpz., 14, 838, (1904).

5. A. Foley and W. Souder, Phys. Rev., 35, 373, (1912).

6. R. J. Strutt, (Lord Rayleigh), Proc. Roy. Soc. A., 183, 26, (1944).

7. H. Zanstra, Proc. Roy. Soc., 186, 236, (1946).

8. R. Lee and R. Fowler, Phys. Rev., 81, 457, (1951), 85, 732, (1952).

9. R. Fowler, J. Goldstein, and B. Clotfelter, Phys. Rev., 82, 879, (1951).

10. R. Fowler, W. Atkinson, and L. Marks, Phys. Rev., 87, 966, (1952).

11. R. Fowler, W. Atkinson, W. Compton, and R. Lee, Phys. Rev., 88, 137, (1952).

12. J. Goldstein, "Anomalous Radiation Processes in Gases other than Hydrogen." Unpublished Master's thesis, University of Oklahoma, (1948).

13. W. Compton, "Investigation of Reflected Luminosity in Pulse Gas Discharges." Unpublished Master's thesis, University of Oklahoma, (1951).

14. R. Lee, "Investigation of Afterglow in Hydrogen Discharges." Unpublished Master's thesis, University of Oklahoma, (1949).

15. B. Clotfelter, "Anomalous Radiation Processes in Pulsed Gas Discharges." Unpublished Master's thesis, University of Oklahoma, (1949).

16. W. Atkinson, "Half Intensity Breadths of the Balmer Lines in Pulsed Gas Discharges." Unpublished Master's thesis, University of Oklahoma, (1950).

17. L. Marks, "Ion Concentration Versus Intensity in Pulsed Gas Discharges." Unpublished Master's thesis, University of Oklahoma, (1951).

18. A. Kleider, "On the Nature of Luminous Fronts in Gas Discharges." Unpublished Master's thesis, University of Oklahoma, (1952).

19. H. Rose, "Ion Concentrations and Recombination in Electrically Excited Shock Tubes." Unpublished Master's thesis, University of Oklahoma, (1952).

20. T. Coleman, "Constrained Spark Expansions from Mechanically Isolated Discharge Chambers." Unpublished Master's thesis, University of Oklahoma, (1952).

21. R. Courant and K. O. Friedrichs, Supersonic Flow and Shock Waves. New York: Interscience Publishers, Inc., (1948).

22. Geiger, Mautz, Hollyer, and Laporte, Engineering Research Institute Report TOIV, University of Michigan, (1949).

23. A. Einstein, Stizb. d. Akad. d. Wien, Berlin, 65, 380, (1920).

24. C. Suits, "High-Temperature Gas Measurements in Arcs," Temperature Its Measurement and Control in Science and Industry. New York: Reinhold Publishing Corporation, (1941).

25. Brinkley, Kirkwood, and Richardson, The Hugoniot Curve for Air from 300° to 1500° C. Report Division 8 NDRC, (1944).

26. E. Resler, S. Lin, and A. Kantrowitz, J. Appl. Phys., 23, 1390, (1952).

27. R. Williamson, Astrophys. J., 103, 139, (1946).

28. J. Denisse and Y. Rocard, J. Phys. Radium, 12, 893, (1951).

29. B. Clotfelter, "Experimental Studies of Transport Phenomena in Highly Ionized Gasses." Unpublished Ph. D. thesis, University of Oklahoma, (1953).

30. G. Lundquist, J. Appl. Phys., 23, 374, (1952).

31. Cassen and Stanton, J. Appl. Phys., 19, 307, (1948).

32. Zeldovich, J. Exp. Theor. Phys. USSR, 4, 363, (1946).

33. I Novikov, Dokl. Akad. Nauk, SSSR 59, 1545, (1948).

34. Liepmann and Pucket, Aerodynamics of a Compressible Fluid. New York: John Wiley & Sons, Inc. (1947).